Journal of Physics D: Applied Physics

Enhancement of extraordinary optical transmission and sensing performance through coupling between metal nanohole and nanoparticle arrays

To cite this article before publication: Bobo Du *et al* 2019 *J. Phys. D: Appl. Phys.* in press https://doi.org/10.1088/1361-6463/ab1835

IOP Publishing Journal Title
Journal **XX** (XXXX) XXXXXX https://doi.org/XXXX/XXXX

Enhancement of extraordinary optical transmission and sensing performance through coupling between metal nanohole and nanoparticle arrays

Bobo Du[1,2], Yuan Yang[1], Yang Zhang[1], Peipei Jia[2,3], Heike Ebendorff-Heidepriem[2,3], Yinlan Ruan[2,3], and Dexing Yang[1]

[1] MOE Key Laboratory of Material Physics and Chemistry under Extraordinary Conditions, and Shaanxi Key Laboratory of Optical Information Technology, School of Science, Northwestern Polytechnical University, Xi'an 710072, China
[2] Institute for Photonics and Advanced Sensing (IPAS) and School of Physical Sciences, The University of Adelaide, Adelaide, South Australia 5005, Australia
[3] ARC Centre of Excellence for Nanoscale BioPhotonics (CNBP), The University of Adelaide, Adelaide, South Australia 5005, Australia

E-mail: yinlan.ruan@adelaide.edu.au, dxyang@nwpu.edu.cn

Received xxxxxx
Accepted for publication xxxxxx
Published xxxxxx

Abstract

The extraordinary optical transmission (EOT) of sub-wavelength nanohole array is significantly enhanced through introducing nanoparticles, including nanospheres and nanocylinders, into the centers of the nanoholes. Maxima of 56% and 48% for nanocylinder and nanosphere matrices are achieved, compared with that of 37% for a none-in-hole nanohole array gold film. The mechanism behind the phenomena is discussed, indicating that surface plasmon mode coupling between nanoholes and nanoparticles rather than Fabry–Pérot resonance is the cause for the EOT enhancement. High near-field intensity enhancement also leads to the interaction between analytes and optical field increasing, therefore an improved sensitivity and figure of merit for biosensing. The modified structures are highly promising in practical sensing applications due to the incident angle independence. Similar results are obtained for a hexagonal array of nanohole gold film and nanoparticle modifications thereof.

Keywords: extraordinary optical transmission, sensing performance, nanohole, nanoparticle

1. Introduction

Greatly enhanced transmission of light, i.e. the extraordinary optical transmission (EOT), through opaque metallic films perforated by nanohole arrays was first observed in 1998 [1, 2] and initiated important further experimental and theoretical work [3-8]. The extraordinary property reflects the transmission of light with orders of magnitude larger than the expected from standard aperture theory [9]. This is attributed to the coupling of light with plasmons on the surface of the patterned metal film, which was found to be controllable by incorporating periodic structures surrounding the subwavelength holes [10], manipulating the array lattice [11], and loading the holes with

different dielectric materials [12]. The enhanced optical transmissions have been demonstrated with other architectures, including nanoslit arrays [3, 13-15], nanoslits covered by metallic nanostrips as nanocavity antennas [16], subwavelength holes blocked by opaque metal disks [17], localized surface plasmon resonance (LSPR) around nanoparticles or nanoparticle arrays [18]. These results led to a flurry of intense theoretical and experimental researches to control optical properties of structured materials. The research enabled ~~aiming at~~ applications in novel photonic devices, such as sun light harvesting [19, 20], surface-enhanced Raman scattering (SERS) [21, 22], sensing [23-30], sub-wavelength integrated optical circuits [31-33], and nanoscale control of light [34-36].

In SERS architectures, ~~In this work, inspired by SERS, where~~ the interaction between individual dipole plasmons can significantly enhance the local electromagnetic fields around nanoparticles by up to $|E|^2 > 10^7$ [37]. Inspired by this, here, we theoretically investigate a new structure by putting gold nano-spheres or -cylinders into holes of the nanohole array gold film to achieve further enhanced EOT. The nanohole gold film shows reliable and reproducible surface plasmon resonance (SPR) properties and is being used for SPR biosensors in-house [38, 39]. Introduction of gold nano-spheres or -cylinders is found to lead to a strong enhancment effect on the electric fields in the arrays, making the structures promising candidates for surface plasmon sensors. We thus demonstrate their potential for label-free biosensing with an improved sensitivity. These structures are promising to be integrated with various platforms, including optical fibers and chip devices, and will attract more applications in novel optoelectronic devices, such as high efficiency optical probes, sensors, enhanced spectroscopy, and solar cells, etc., which will benefit from the enhanced electrical fields and EOT.

2. Structures and simulation

A three-dimensional (3D) finite-difference time-domain (FDTD) method (FDTD solutions, Lumerical Solutions Inc.) was used to simulate the transmission. ~~through a~~ A square and a hexagonal array of nanohole gold films ~~for comparison~~ are compared on a transparent substrate (fused silica, 1.45 refractive index), respectively, with three configurations: (i) the holes are open without any modification (none in hole), (ii) the holes are modified with gold sphere with a diameter of d_s at the center (sphere in hole), (iii) the holes are modified with gold cylinders with a diameter of d_c and fixed height of 100 nm (cylinder in hole), as shown in Fig. 1. The thickness of the gold film is fixed as 100 nm, which makes sure that the unperforated gold film is opaque to light [4] but not too thick for surface plasmon propagation since plasmon attenuates dramatically with the thickness increasing [1]. The period P and nanohole diameter D will be analyzed in the following sections.

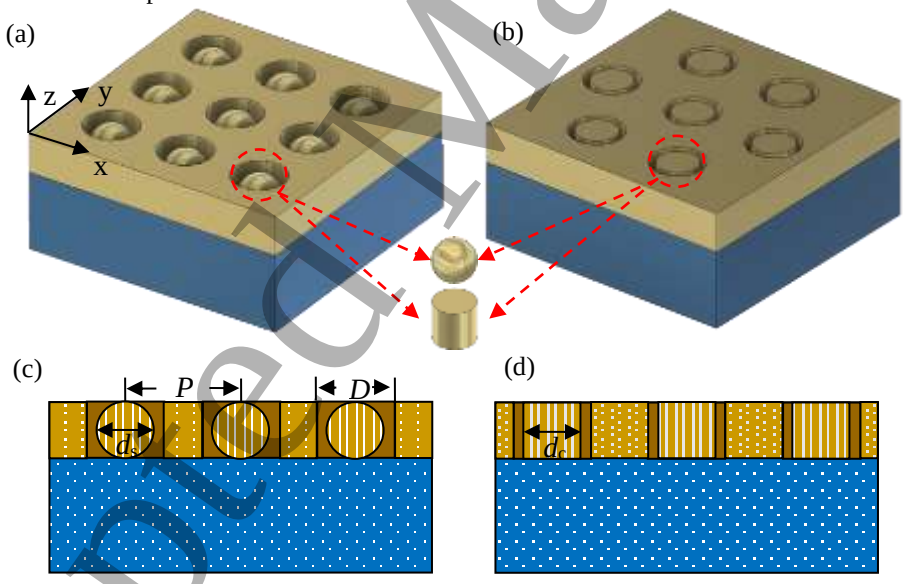

Fig. 1. Schematic diagram of the proposed structures. A square (a) and a hexagonal (b) array of nanohole gold films are modified by nanocylinders and nanospheres at the hole centers, respectively. The array period and hole diameter are kept as the same in the two array matrices for comparison.

In the simulation, the structures are illuminated by a normal plane wave along the z-axis with polarization direction along the x-axis. Periodic boundary conditions are set in x- and y-directions, while along the z-axis perfect matched layer (PML) boundary condition is used to minimize unnecessary boundary reflections. The dielectric permittivity data obtained by Johnson and Christy [41] are used for the gold film. The whole structure is surrounded by dielectric environment of vacuum. Transmission spectra are monitored to investigate the optical properties in detail. In addition, in our work, we focus on the transmission intensity for EOT and the resonance wavelength for sensing. Thus, the optimized multi-coefficient model fit of

the material dielectric constants are conducted and a broadband light source is used to ensure a basically flat profile within the band of interest. These guarantee the minimized simulation error in the wide band.

3. Results and discussions

First, we discuss the transmission characteristics of the nanohole arrays without nanoparticle modifications (none in hole). Note that in the following main body, we only discuss a square array of nanohole gold film and the modifications thereof, and details about a hexagonal array could be found in the appendix.

Figure 2 shows the transmission spectra of a square array of nanohole gold films. ~~Surface plasmon resonance (~~SPR~~)~~ peaks can be clearly identified in these spectra. The single peak at 500 nm comes from direct light transmission through the gold film, which could be attributed to the interaction between the conduction band and the *d*-band of Au [41] and is independent of the geometric structure as marked by the arrows in Figs. 2(a) and 2(b). The transmission minimum at the left (short wavelength) side of each maximum in all cases with different periods and diameters is associated with Wood's anomaly due to the light diffracted parallel to the Au surface and thus could not be transmitted [42].

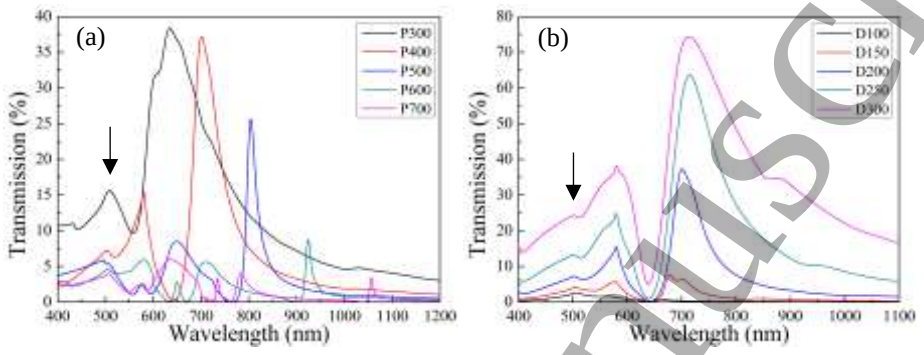

Fig. 2. Transmission spectra of the none-in-hole structures with (a) varying array periods *P* at fixed 200 nm hole diameter and (b) varying hole diameters *D* at fixed 400 nm array period.

As shown in Fig. 2(a), systematic trends in the transmission spectra as a function of period from 300 to 700 nm are evident, namely, the λ_{max} of the dominant resonance redshifts from around 650 to 1050 nm, the overall transmission decreases, and the transmission peaks narrow as the period of the array is increased. The transmission peaks result from surface plasmons on a two-dimensional lattice, which can be described by the dispersion relation [4]

$$\lambda_{max}(i,j) = \frac{P}{\sqrt{i^2+j^2}}\sqrt{\frac{\varepsilon_m \varepsilon_d}{\varepsilon_m+\varepsilon_d}}, \quad (1)$$

where P is the period of the array, i and j are integers corresponding to Bragg-type scattering modes, ε_m is the real part of the complex dielectric function of the metal, and ε_d is the dielectric constant of the substrate, fused silica. The redshifts of these transmission peaks with increasing period of the array at a fixed hole diameter of 200 nm are evident with Eq. (1). The decrease in overall transmission in Fig. 2(a) is due to the decreasing apertures area ratios when the period increases. Figure 2(b) presents the dependence of the transmission on the hole size (diameter *D* from 100 to 300 nm) with a fixed period of 400 nm. As expected, the maxima (~580 and 700 nm) and minimum (~638 nm) are located at the same wavelengths [2, 4], but the overall transmission increases with increasing *D*. This result is also attributed to increasing apertures area ratio as for the results for varying periods. With 200 nm hole diameter, the maximum transmission 37% at around 700 nm compared with 19% of the aperture area ratio is obtained~~.~~. The normalized-to-the-area transmission exceeds unity, indicating for the none-in-hole structure, ~~nearly two times higher transmission (~~EOT~~)~~ is obtained. Note that the resonance peak around 700 nm broadens significantly as the diameter increases (Fig. 2(b)). For specific applications such as sensing, high transmission and narrow bandwidth are desirable in order to achieve high signal-to-noise ratio and low detection limit, respectively. Therefore, 400 nm array period and 200 nm hole diameter for the none-in-hole structure with medium transmission and bandwidth are selected to demonstrate further enhancement effects on the transmission and potential sensing performance through modifications of nanoparticles.

Figure 3 depicts the spectra for the two modified architectures, i.e. cylinder-in-hole (Fig. 3(a)) and sphere-in-hole (Fig. 3(b)), based on fixed square array of nanohole gold film of 100 nm thickness, 400 nm period, and 200 nm diameter.

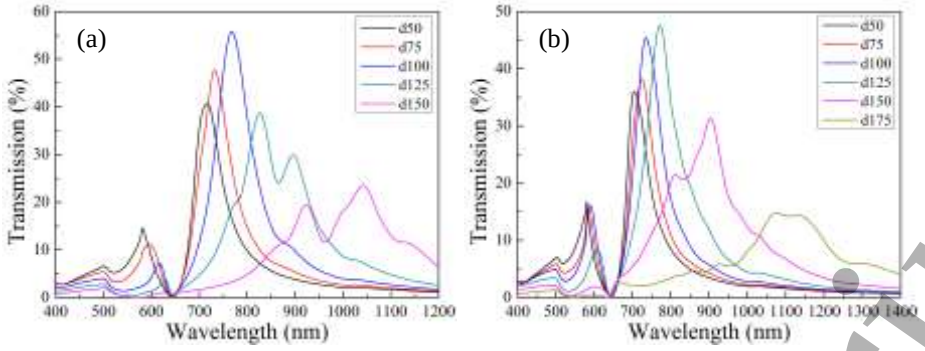

Fig. 3. Transmission spectra for nanohole array gold films with 100 nm thickness, 400 nm period, and 200 nm diameter modified by different diameters of (a) cylinders and (b) spheres.

It can be seen that similar trends are observed in both cases. With the increase of the particle diameter from 50 to 100 nm for cylinder-in-hole and 50 to 125 nm for sphere-in-hole structures, the maximum peak transmission rises at first due to increased effective coupling between a localized mode (specifically, the TE_{11} mode supported by the individual aperture) and the surface plasma polaritons of the metal-dielectric interfaces with a periodicity [43, 44]. However, for larger particles, the transmission drops, which is the result of the fact that the metal loss becomes dominant as the particle diameters increase [45]. Thus, maximum transmission can be obtained with a cylinder of 100 nm diameter and a sphere of 125 nm diameter modified nanohole array gold film, respectively.

In addition, as the particle diameters increase, the transmission peaks show a redshift and broadening. This is attributed to the secondary radiation enhancement, where electrons lose energy experiencing a damping effect.~~, which~~ The damping effect makes the SPR peaks broad, red-shifted, and asymmetric [46].

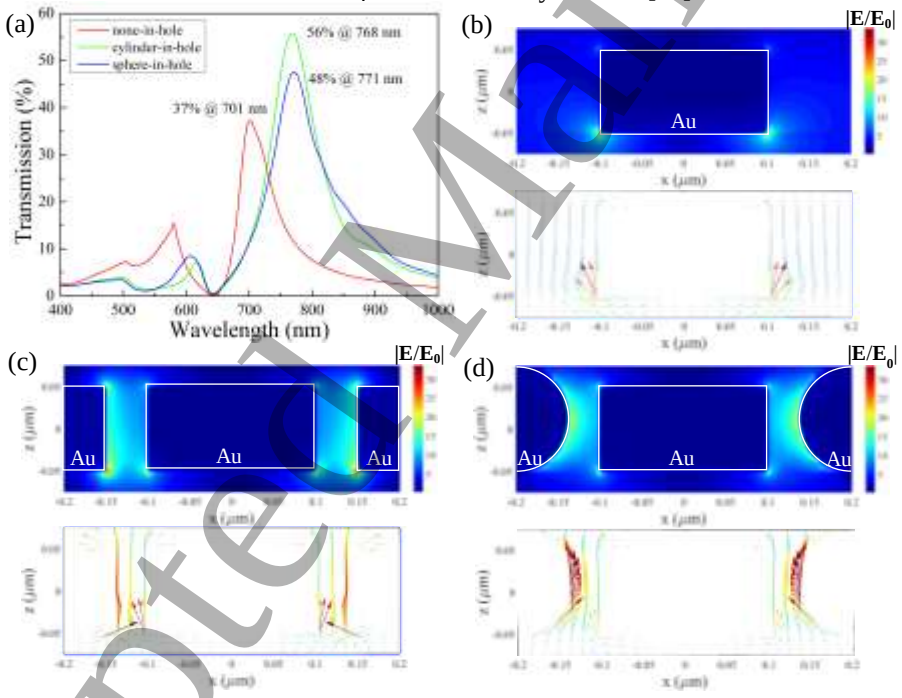

Fig. 4. Further enhanced EOT with cylinder and sphere modifications. (a) transmission spectra, and the electric field (Up) and Poynting vector (Down) distributions for the three structures (b) none-in-hole at 701 nm, (c) cylinder-in-hole at 768 nm, and (d) sphere-in-hole at 771 nm.

Figure 4(a) summarizes the transmission spectra of the two modifed structures with maximum EOT and the spectrum of the none-in-hole film. It can be seen that the two modified structures show both higher peak transmissions and longer wavelengths than the none-in-hole structure. For the none-in-hole film, 37% transmission is observed at 701 nm, while for cylinder- and sphere-in-hole structures, further enhanced transmission of 56% and 48% are observed at 768 and 771 nm, respectively, even though the open aperture area within each nanohole is reduced because of the introduction of nanoparticles. ~~The mechanism behind this is as mentioned above, which is in contrast to the mechanism suggested in [37,~~

~~38], where Waele *et al.* and Ni *et al.* concluded that Fabry-Pérot (FP) resonant cavity effect was responsible for the EOT phenomena in the structure of metal films perforated with hole arrays.~~

To verify and reveal the origin of the enhanced EOT, electric field and Poynting vector distributions are simulated at each wavelength of maxima on a vertical cross section for the three matrices and presented in Figs. 4(b)-4(d). No standing wave is observed along the nanohole channels in all the three cases, which means no FP effect observed here [44]. This is in contrast to the mechanism suggested in [47, 48], where Waele *et al.* and Ni *et al*. concluded that Fabry-Pérot (FP) resonant cavity effect was responsible for the EOT phenomena in the structure of metal films perforated with hole arrays. Compared with the electric field mostly confined at the bottom corners of the none-in-hole array, strong electric field enhancements are observed at the top and bottom corners of not only the nanoholes but also the nanoparticles as well as their gaps in both cylinder and sphere modified structures. Also, the Poynting vector profiles clearly show that there are intensive optical energy exchanges among nanoparticles and nanoholes, which indicates that the nanoparticles act as nano-antennas collecting the incident light through the coupling between the modes of nanohole and particles and then re-emitting it into the free-space.~~, which~~ This contributes to the further enhanced EOT for particle modified arrays. The difference of the transmissions for cylinder and sphere modifications could also be attributed to the electric field distribution differences. The cylinder induces stronger transmission enhancement than the sphere does because more electric field is concentrated in the middle gap between the sphere and the nanohole as shown in Fig. 4(d), which is not the most efficient path to re-emit optical waves.

It is possible to have a small amount of displacement from the centers of nanoholes caused by the fabrication processe. It is found that our structures can tolerate a small divergence in fabrication accuracy. 5 nm offset of the nanoparticles away from the nanohole centers only induces about 2% reduction in the transmissions with square arrays (not shown here). In addition, to date, sub-5 nm features and sub-nanometer position accuracy have been achieved by the most frequently used top-down fabrication methods for plasmonic devices, electron-beam lithography (EBL) and focused ion beam (FIB) techniques [49, 50]. These enable the high accuracy fabrication of our structures.

The enhanced electric field could lead to a stronger interaction between analytes and the optical field, namely the interaction volume, offering an improved sensitivity for refractive index (RI) change of sensing media. To evaluate the effect of the particle modifications on RI sensing performance, we perform the aqueous RI sensing by assuming a label-free biosensing case, where the bulk RI, n_s, is tuned by changing the bovine serum albumin (BSA) concentration, which can be mathematically expressed as [51]

$$n_s = n_C + C \cdot \frac{dn}{dC}, \quad (2)$$

where n_C is the RI of the buffer solution, herein 1.3330 of water is assumed, C is the concentration of BSA, and dn/dC is the increment in RI due to the concentration alteration. The refractive index increment parameter is dn/dC=0.17 cm^3/g, in the case of BSA solutions.

Characteristics that are commonly used to evaluate the performance of RI sensors are sensitivity (defined as $S=\Delta\lambda/\Delta n_s$, where $\Delta\lambda$ is the shift in resonance wavelength due to a change Δn_s of sensing medium's RI.), and a figure of merit (FOM, calculated as S/FWHM, full width at half maximum).

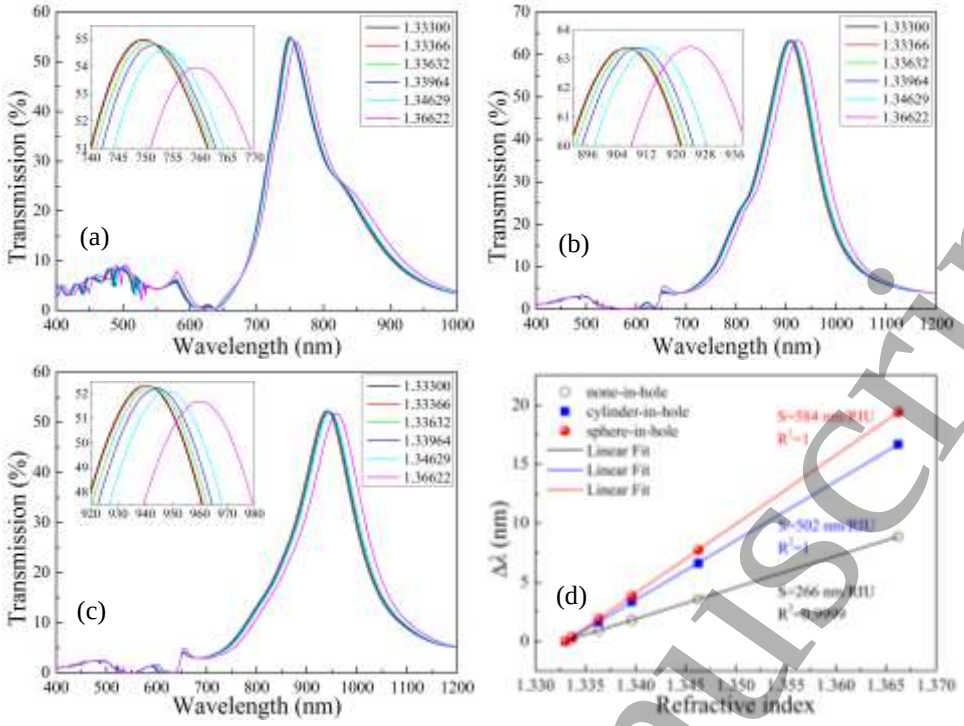

Fig. 5. (a) Transmission spectra for the three structures investigated (a) none-in-hole, (b) cylinder-in-hole, and (c) sphere-in-hole for different n_s, and (d) the sensitivities of these three structures.

Figure 5 shows the transmission spectra and sensitivities as a function of n_s for the three structures investigated as shown in Figs. 4(b)-4(d), where the concentrations of BSA solutions are 0, 10, 50, 100, 200, and 500 μM, corresponding to RIs of 1.33300, 1.33366, 1.33632, 1.33964, 1.34629, and 1.36622, respectively. The insets in Figs. 5(a)-5(c) are the corresponding zoom-in curves at each maximum. As shown in Fig. 5, the peak wavelengths exhibit a redshift as the RI increases, and spectral analysis shows that the relationship between the wavelength shift and the RI is consistent with a linear fit. Both the structures with the cylinder and sphere modifications offer around twice higher sensitivities compared with that of none-in-hole array film. More specifically, the none-in-hole array has a sensitivity of 266 nm/RIU (refractive index unit), while the cylinder modification gives rise to an enhanced sensitivity of 502 nm/RIU and the sphere modification shows a highest sensitivity of 584 nm/RIU. The increase in sensitivity is the result of the much larger sensing volume offered by the nanoparticle modified architecture, i.e. more electric field is emitted and the interaction between analytes and the optical field increases, while for the sphere-in-hole structure the electric field almost overlaps with the analytes within the whole hole as shown in Fig. 4(d), associated with the largest interaction volume, therefore a highest sensitivity [52].

The obtained FWHMs for none-, cylinder-, and sphere-in-hole architectures are 91, 124, and 128 nm, and the corresponding FOMs are 2.9, 4.0, and 4.6, respectively. It indicates that the sphere modification takes advantage over the cylinder modification in terms of the sensitivity and FOM. There are usually two approaches adopted to achieve high FOM: (i) decrease the FWHM of the peak, and (ii) increase the sensitivity. Due to the limitation of the operation wavelength range of spectrometer, it is more desirable to obtain a high FOM with an appropriate sensitivity for RI sensors, i.e., minimize the FWHM. The period and diameter of the nanohole array could be carefully tuned and optimized to achieve a narrow FWHM, as shown in Fig. 2. Also, Fano resonance is an effective approach to decrease the FWHM of SPR dips or peaks [23, 53].

More interestingly, the resonance peak positions of the modified structures do not change with the incident angle of illumination, as illustrated in Fig. 6, which might be attributed to the property of TE_{11} mode, i.e. the position of TE_{11} mode is directly connected to the geometric prarameters of the nanohole and independent on the incident angle of illumination [44]. This feature makes these structures ideal for sensing shown above and other applications where angle independence is important [54].

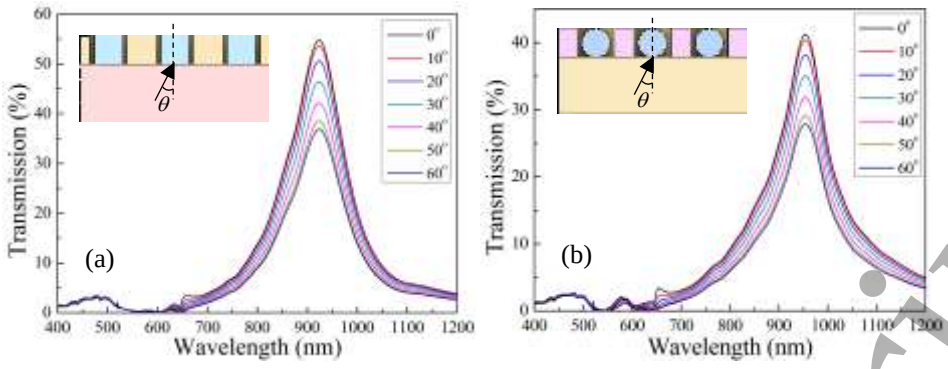

Fig. 6. The angular dependences on the transmission resonances of (a) cylinder-in-hole and (b) sphere-in-hole architectures.

In addition, similar results are obtained for a hexagonal array of nanohole gold film and the nanoparticle modifications thereof (see appendix for detail), as summarized in Table 1, where maxima of 55% and 50% are achieved by introducing nanocylinders and nanospheres, respectively. The cylinder-in-hole results in 490 nm/RIU sensitivity and 3.3 FOM, while the sphere-in-hole results in 581 nm/RIU sensitivity and 3.8 FOM. Therefore, square and hexagonal arrays of nanohole modified by particles, including cylinder and sphere, are considered to be good candidates for high-transmission devices and biosensing applications. Especially, the sphere modification based on a square array of nanohole metal film is better for biosensing applications with higher sensitivity and FOM.

Note that the optical transmission and sensing performances might be further enhanced by infiltrating the nanoholes with gain media, where gain media are able to compensate the dissipative losses via the energy transfer from gain media to metal nanostructures [35, 55].

Table 1. Summary of Transmission and Sensing Performances for Square and Hexagonal Arrays of Metal Nanohole and Modifications thereof

Array	Modification	Maximum (%)	Sensitivity (nm/RIU)	FWHM (nm)	FOM
Square	None	37	266	91	2.9
	Cylinder	56	502	124	4.0
	Sphere	48	584	128	4.6
Hexagonal	None	36	234	104	2.3
	Cylinder	55	490	149	3.3
	Sphere	50	581	153	3.8

4. Conclusion

Further enhanced EOT with maxima of 56%, and 48% are achieved by introducing nanocylinders and nanospheres in the centers of nanoholes of a square array, respectively. Mode coupling between nanoholes and nanoparticles rather than FP resonance is attributed to the enhancement, which is verified by the electric field distribution through FDTD simulation. Due to the high near-field intensity enhancement, the interaction volume between analytes and the optical field increases, leading to improved sensitivities and FOM (502 nm/RIU with FOM of 4.0 for cylinder matrix and 584 nm/RIU with FOM of 4.6 for sphere matrix). Compared with a hexagonal nanohole array gold film and the nanoparticle modifications thereof, the square array of nanohole modified by nanocylinder offers highest transmission, while the sphere modification based on a square array of nanohole metal film is better for biosensing applications with higher sensitivity and FOM. The promising optical property will attract more applications in novel optoelectronic devices.

Acknowledgements

This work is funded by the Innovation Foundation for Doctor Dissertation of Northwestern Polytechnical University (CX201818). The authors would like to acknowledge the support of the ARC Centre of Excellence for Nanoscale BioPhotonics (CNBP). Bobo Du gratefully acknowledges the financial support from the China Scholarship Council.

Appendix. Enhancement of EOT and sensing performance for a hexagonal metal array of nanohole and the nanoparticle modifications thereof

Figure A1 shows the transmission spectra of a hexagonal array of nanohole gold film. The transmission peaks result from surface plasmons on a two-dimensional lattice, which can be described by the dispersion relation [4]

$$\lambda_{\max}(i,j)=\frac{P}{\sqrt{\frac{3}{4}\left(i^2+ij+j^2\right)}}\sqrt{\frac{\varepsilon_m\varepsilon_d}{\varepsilon_m+\varepsilon_d}}, \qquad (A.1)$$

where P is the period of the array, i and j are integers corresponding to Bragg-type scattering modes, ε_m is the real part of the complex dielectric function of the metal, and ε_d is the dielectric constant for the dielectric. 400 nm period and 200 nm hole diameter are selected, where the maximum transmission is 36% at 655 nm compared with 23% of the aperture area ratio.

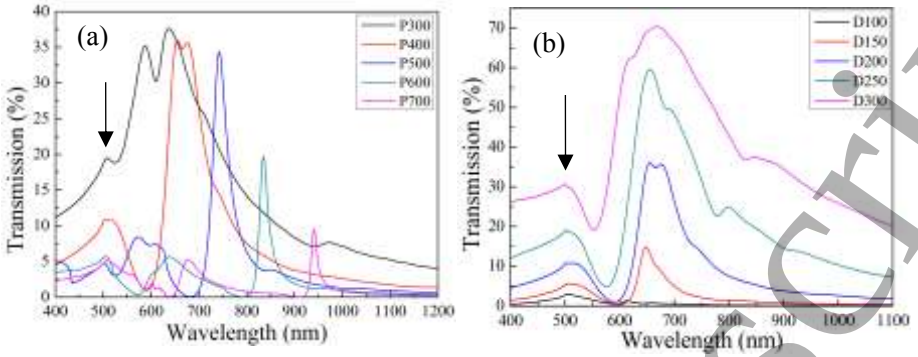

Fig. A1. Transmission spectra of the none-in-hole structures with (a) varying hexagonal array periods P at a fixed 200 nm hole diameter and (b) varying hole diameters D at a fixed 400 nm array period.

Figure A2 depicts the spectra for the two modified architectures, i.e. cylinder-in-hole (Fig. 7(a)) and sphere-in-hole (Fig. 7(b)), based on a fixed nanohole array gold film of 100 nm thickness, 400 nm period, and 200 nm diameter.

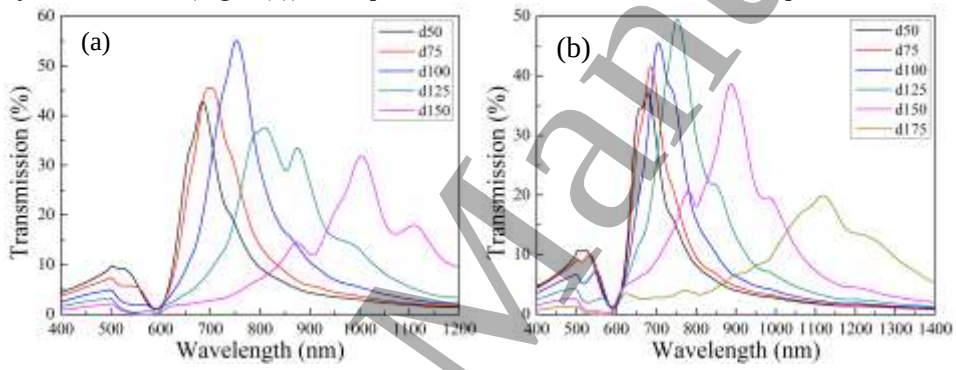

Fig. A2. Transmission spectra for nanohole array gold films with 100 nm thickness, 400 nm period, and 200 nm diameter modified by different diameters of (a) cylinders and (b) spheres.

Similar trends are observed in both cases. With the increase of the modification particle diameter, the maximum peak transmission rises at first, but then the transmission drops for larger particle diameters. Also, with the particle diameters increasing, the transmission shows a redshift and broadening. Maximum transmission is obtained with a cylinder of 100 nm diameter and a sphere of 125 nm diameter modified nanohole array gold film, respectively.

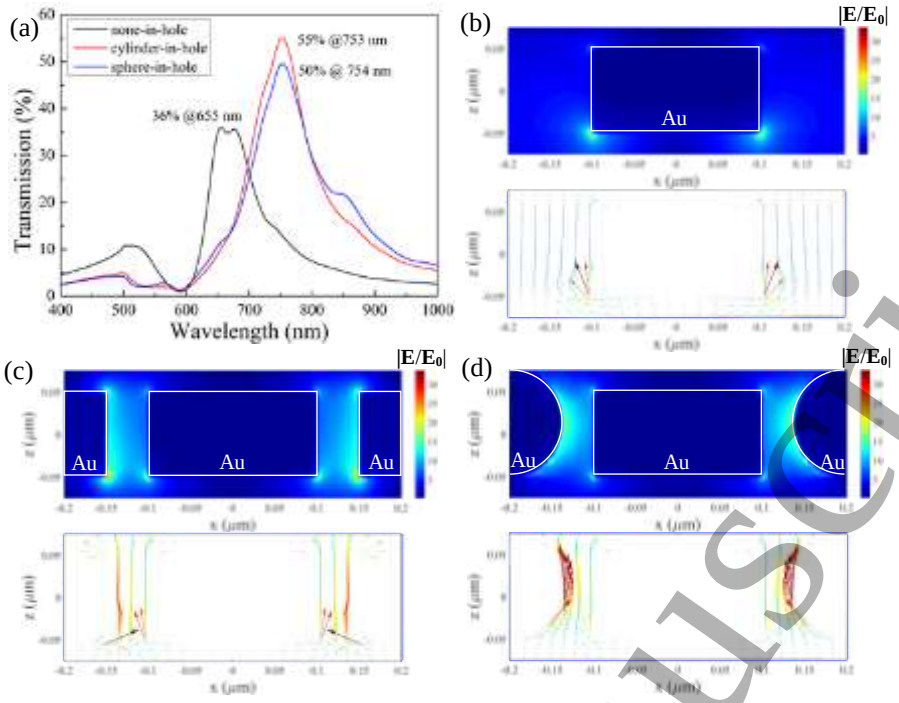

Fig. A3. Further enhanced EOT with cylinder and sphere modified. (a) transmission spectra, and the electric field (Up) and Poynting vector (Down) distributions for (b) none-in-hole at 655 nm, (c) cylinder-in-hole at 753 nm, and (d) sphere-in-hole at 754 nm.

Figure A3 shows the further enhanced EOT due to cylinder and sphere modifications. The two modified structures show both higher peak transmission and longer wavelengths than the none-in-hole array. 36% transmission is observed at 655 nm for the none-in-hole film, while for cylinder- and sphere-in-hole architectures, further enhanced transmission of 55% and 50% are observed at 753 and 754 nm, respectively. Also, the electric field distributions reveal that the FP resonant cavity effect plays no role in the further EOT phenomena. And the Poynting vector profiles indicates that the nanoparticles act as nano-antennas collecting the incident light through the coupling between the modes of nanohole and particles and then re-emitting it into the free-space, which contributes to the further enhanced EOT for particle modified arrays.

Note that an around 10% reduction in the transmissions is induced due to 5 nm offset of the nanoparticles away from the nanohole centers with hexagonal arrays (not shown here). The larger reduction than those with square arrays is attributed to the effect that with fixed period, the hexagonal arrays have higher nanostructure densities than the square arrays, where neighbouring modes are more likely to interact with each other with hexagonal arrays [56]. Therefore, the geometrical change (i.e. offset here) in the hexagonal array nanostructures has a larger influence on the resonance behaviors. However, all the transmissions are still higher than those of the unmodified structures (about 36%). Thus, our structures can tolerate a small divergence caused by either EBL or FIB techniques.

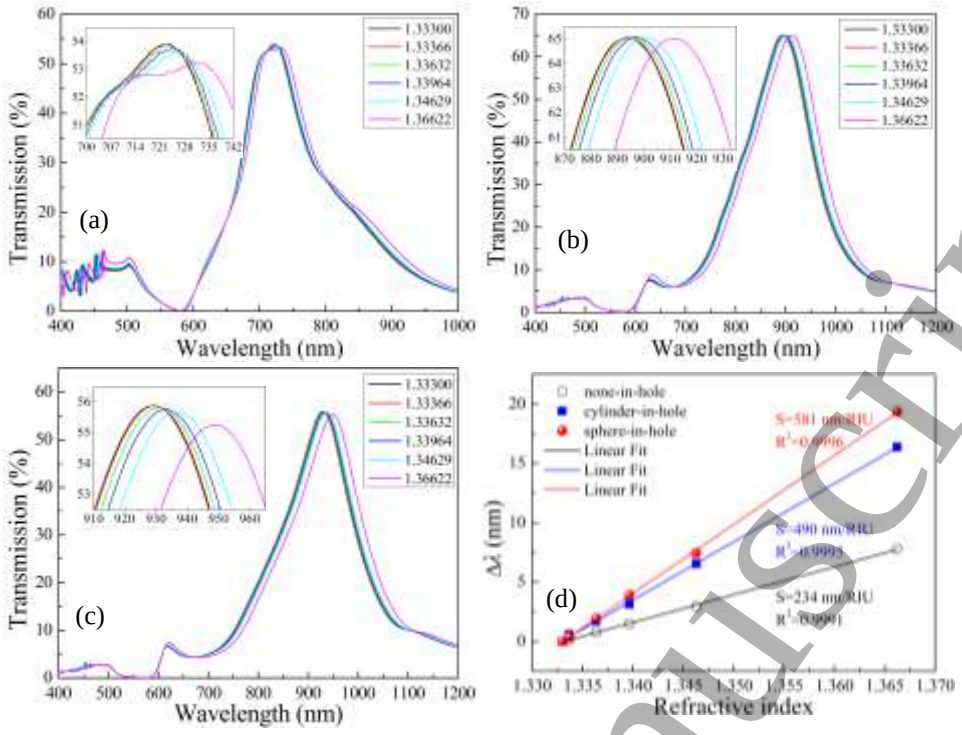

Fig. A4. Transmission spectra for the three structures investigated (a) none-in-hole, (b) cylinder-in-hole, and (c) sphere-in-hole for different n_s, and (d) the sensitivities of these three structures.

Figure A4 shows the transmission spectra and sensitivities for BSA RI sensing. The peak wavelengths exhibit a redshift as the RI increases. Both the structures with the cylinder and sphere modifications offer higher sensitivities and FOM (490 nm/RIU sensitivity and 3.3 FOM for cylinder-in-hole structure and 581 nm/RIU sensitivity and 3.8 FOM for sphere-in-hole structure, respectively), compared with 234 nm/RIU sensitivity and 2.3 FOM for none-in-hole film. The corresponding FWHMs are 104, 149, and 153 nm, respectively.

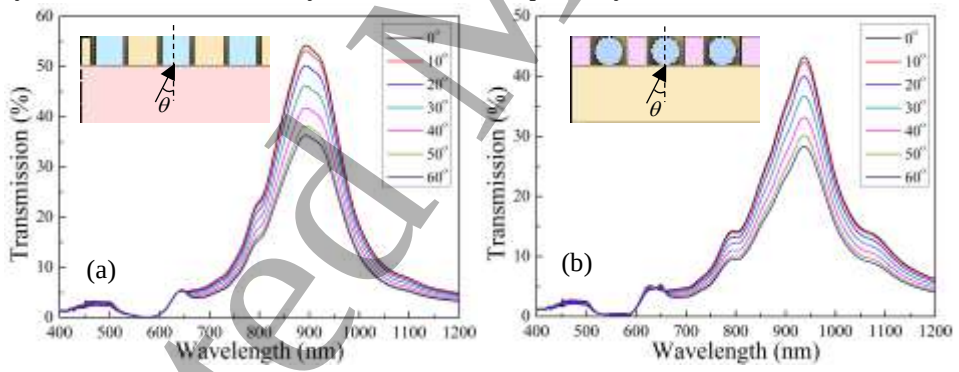

Fig. A5. The angular dependences on the transmission resonances of (a) cylinder-in-hole and (b) sphere-in-hole architectures.

The resonance peak positions of the modified structures are independent on the incident angle of illumination, as shown in Fig. A5.

References

[1] T. W. Ebbesen, H. J. Lezec, T. Ghaemi, and P. A. Wolff, "Extraordinary optical transmission through sub-wavelength hole arrays," Nature **391**, 667–669 (1998)

[2] H. F. Ghaemi, T. Thio, D. E. Grupp, T. W. Ebbesen, and H. J. Lezec, "Surface plasmons enhance optical transmission through subwavelength holes," Phys. Rev. B **58**(11), 6779–6782 (1998).

[3] U. Schröter and D. Heitmann, "Surface-plasmon-enhanced transmission through metallic gratings," Phys. Rev. B **58**(23), 15419–15421 (1998).

[4] T. Thio, H. F. Ghaemi, H. J. Lezec, P. A. Wolff, and T. W. Ebbesen, "Surface-plasmon-enhanced transmission through hole arrays in Cr films," J. Opt. Soc. Am. B **16**(10), 1743-1748 (1999).

[5] L. Martín-Moreno, F. J. García-Vidal, H. J. Lezec, K. M. Pellerin, T. Thio, J. B. Pendry, and T. W. Ebbesen, "Theory of extraordinary optical transmission through subwavelength hole arrays," Phys. Rev. Lett. **86**(6), 1114– 1117 (2001).

[6] H. Liu, and P. Lalanne, "Microscopic theory of the extraordinary optical transmission," Nature **452**, 728-731 (2008).

[7] H. J. Lezec, A. Degiron, E. Devaux, R. Linke, L. Martin-Moreno, F. Garcia-Vidal, and T. Ebbesen, "Beaming light from a subwavelength aperture," Science **297**, 820-822 (2002).

[8] R. Dhama, V. Caligiuri, L. Petti, A. R. Rashed, M. Rippa, R. Lento, R. Termine, H. Caglayan, and A. De Luca, "Extraordinary Effects in Quasi-Periodic Gold Nanocavities: Enhanced Transmission and Polarization Control of Cavity Modes," ACS Nano **12**, 504-512 (2018).

[9] H. A. Bethe, "Theory of diffraction by small holes," Phys. Rev. **66**(7–8), 163–182 (1944).

[10] F. Garcia-Vidal, E. Moreno, J. Porto, and L. Martin-Moreno, "Transmission of light through a single rectangular hole," Phys. Rev. Lett. **95**, 103901 (2005).

[11] G. Ctistis, P. Patoka, X. Wang, K. Kempa, and M. Giersig, "Optical transmission through hexagonal arrays of subwavelength holes in thin metal films," Nano Lett. **7**(9), 2926–2930 (2007).

[12] K. J. Webb and J. Li, "Analysis of transmission through small apertures in conducting films," Phys. Rev. B **73**, 033401 (2006).

[13] J. A. Porto, F. J. Garcia-Vidal, and J. B. Pendry, "Transmission resonances on metallic gratings with very narrow slits," Phys. Rev. Lett. **83**(14), 2845–2848 (1999).

[14] Y. Ye and Y. Jin, "Enhanced transmission of transverse electric waves through subwavelength slits in a thin metallic film," Phy. Rev. E **80**, 036606 (2009).

[15] S. Kim, M. S. Jang, V. W. Brar, Y. Tolstova, K. W. Mauser, and H. A. Atwater, "Electronically tunable extraordinary optical transmission in graphene plasmonic ribbons coupled to subwavelength metallic slit arrays," Nat Commun **7**, 12323 (2016).

[16] Y. Cui, and S. He, "Enhancing extraordinary transmission of light through a metallic nanoslit with a nanocavity antenna," Opt. Lett. **34**, 16-18 (2009).

[17] W. Li, J. Hu, and S. Chou, "Extraordinary light transmission through opaque thin metal film with subwavelength holes blocked by metal disks," Opt. Express **19**, 21098-21108 (2011).

[18] E. Hao and G. C. Schatz, "Electromagnetic fields around silver nanoparticles and dimers," J. Chem. Phys. **120**(1), 357–366 (2004).

[19] Q. Gan, F. J. Bartoli, and Z. H. Kafafi, "Plasmonic-Enhanced Organic Photovoltaics: Breaking the 10% Efficiency Barrier," Adv. Mater. **25**(17), 2385–2396 (2013).

[20] S. E. Han and G. Chen, "Optical absorption enhancement in silicon nanohole arrays for solar photovoltaics," Nano Lett. **10**(3), 1012–1015 (2010).

[21] N. Félidj, J. Aubard, G. Levi, J. R. Krenn, A. Hohenau, G. Schider, A. Leitner, and F. R. Aussenegg, "Optimized surface-enhanced Raman scattering on gold nanoparticle arrays," Appl. Phys. Lett. **82**(18), 3095–3097 (2003).

[22] X. Zhu, L. Shi, M. S. Schmidt, A. Boisen, O. Hansen, J. Zi, S. Xiao, and N. A. Mortensen, "Enhanced Light-Matter Interactions in Graphene-Covered Gold Nanovoid Arrays," Nano Lett. **13**(10), 4690–4696 (2013).

[23] Y. Shen, J. Zhou, T. Liu, Y. Tao, R. Jiang, M. Liu, G. Xiao, J. Zhu, Z.-K. Zhou, X. Wang, C. Jin, and J. Wang, "Plasmonic gold mushroom arrays with refractive index sensing figures of merit approaching the theoretical limit," Nat. Commun. **4**(1), 2381 (2013).

[24] A. V. Kabashin, P. Evans, S. Pastkovsky, W. Hendren, G. A. Wurtz, R. Atkinson, R. Pollard, V. A. Podolskiy, and A. V. Zayats, "Plasmonic nanorod metamaterials for biosensing," Nat. Mater. **8**(11), 867–871 (2009).

[25] P. Jia, and J. Yang, "Integration of large-area metallic nanohole arrays with multimode optical fibers for surface plasmon resonance sensing," Appl. Phys. Lett. **102**(24), 243107-243107-3 (2013).

[26] A. G. Brolo, R. Gordon, B. Leathem, and K. L. Kavanagh, "Surface plasmon sensor based on the enhanced light transmission through arrays of nanoholes in gold films," Langmuir **20**(12), 4813–4815 (2004).

[27] E. Hutter, and J. H. Fendler, "Exploitation of Localized Surface Plasmon Resonance," Adv. Mater. **16**, 1685-1706 (2004).

[28] M. E. Stewart, C. R. Anderton, L. B. Thompson, J. Maria, S. K. Gray, J. A. Rogers, and R. G. Nuzzo, "Nanostructured plasmonic sensors," Chem. Rev. **108**, 494-521 (2008).

[29] T. Yang and H. P. Ho, "Computational investigation of nanohole array based SPR sensing using phase shift," Opt. Express **17**, 11205-11216 (2009).

[30] B. Liu, S. Chen, J. Zhang, X. Yao, J. Zhong, H. Lin, T. Huang, Z. Yang, J. Zhu, and S. Liu, "A Plasmonic Sensor Array with Ultrahigh Figures of Merit and Resonance Linewidths down to 3 nm," Adv. Mater. **30**, 1706031 (2018).

[31] S. Shinada, J. Hashizume, and F. Koyama, "Surface plasmon resonance on microaperture vertical-cavity surface-emitting laser with metal grating," Appl. Phys. Lett. **83**, 836-838 (2003).

[32] W. L. Barnes, A. Dereux, and T. W. Ebbesen, "Surface plasmon subwavelength optics," Nature **424**, 824 (2003).

[33] J. Hashizume, and F. Koyama, "Plasmon-enhancement of optical near-field of metal nanoaperture surface-emitting laser," Appl. Phys. Lett. **84**, 3226-3228 (2004).

[34] E. Ozbay, "Plasmonics: merging photonics and electronics at nanoscale dimensions," Science **311**, 189-193 (2006).

[35] O. Hess, and K. L. Tsakmakidis, "Metamaterials with quantum gain," Science **339**, 654-655 (2013).

[36] K. L. Tsakmakidis, O. Hess, R. W. Boyd, and X. Zhang, "Ultraslow waves on the nanoscale," Science **358** (2017).

[37] S. Zou, and G. C. Schatz, "Silver nanoparticle array structures that produce giant enhancements in electromagnetic fields," Chem. Phys. Lett. **403**, 62-67 (2005).

[38] P. Jia, H. Jiang, J. Sabarinathan, and J. Yang, "Plasmonic nanohole array sensors fabricated by template transfer with improved optical performance," Nanotechnology **24**, 195501 (2013).

[39] P. Jia, and J. Yang, "A plasmonic optical fiber patterned by template transfer as a high-performance flexible nanoprobe for real-time biosensing," Nanoscale **6**, 8836 (2014).

[40] P. B. Johnson and R. W. Christy, "Optical constants of the noble metals," Phys. Rev. B **6**, 4370–4379 (1972).

[41] J. M. McMahon, J. Henzie, T. W. Odom, G. C. Schatz, and S. K. Gray, "Tailoring the sensing capabilities of nanohole arrays in gold films with Rayleigh anomaly-surface plasmon polaritons," Opt. Express **15**, 18119-18129 (2007).

[42] R. W. Wood, "Anomalous diffraction grating," Phys. Rev. **48**(12), 928–936 (1935).

[43] W. J. Fan, S. Zhang, B. Minhas, K. J. Malloy, and S. R. J. Brueck, "Enhanced infrared transmission through subwavelength coaxial metallic arrays," Phys. Rev. Lett. **94**(3), 033902 (2005).

[44] W. Jia, X. Liu, "Mechanism of the superenhanced light transmission through 2D subwavelength coaxial hole arrays," Phys. Lett. A, **344** (6), 451-456 (2005).

[45] J.-S. Huang, T. Feichtner, P. Biagioni, and B. Hecht, "Impedance matching and emission properties of nanoantennas in an optical nanocircuit," Nano Lett. **9**(5), 1897–1902 (2009).

[46] C. Noguez, "Surface plasmons on metal nanoparticles: The influence of shape and physical environment," J. Phys. Chem. C **111**(10), 3806–3819 (2007).

[47] R. De Waele, S. P. Burgos, A. Polman, and H. A. Atwater, "Plasmon dispersion in coaxial waveguides from single-cavity optical transmission measurements," Nano Lett. **9**, 2832-2837 (2009).

[48] H. Ni, M. Wang, T. Shen, and J. Zhou, "Self-assembled large-area annular cavity arrays with tunable cylindrical surface plasmons for sensing," ACS Nano **9**(2), 1913–1925 (2015).

[49] V. Dubois, S. J. Bleiker, G. Stemme, and F. Niklaus, "Scalable Manufacturing of Nanogaps," Adv. Mater. **30**, e1801124 (2018).

[50] L. Bruchhaus, P. Mazarov, L. Bischoff, J. Gierak, A. D. Wieck, and H. Hövel, "Comparison of technologies for nano device prototyping with a special focus on ion beams: A review," Applied Physics Reviews **4**, 011302 (2017).

[51] B. Du, Y. Yang, Y. Zhang, and D. Yang, "SPR Label-Free Biosensor with Oxide-Metal-Oxide-Coated D-Typed Optical Fiber: a Theoretical Study," Plasmonics, 1-7 (2018).

[52] A. Shalabney and I. Abdulhalim, "Sensitivity enhancement methods for surface plasmon sensors," Laser Photonics Rev. **5**(4), 571–606 (2011).

[53] A. E. Miroshnichenko, S. Flach, and Y. S. Kivshar, "Fano resonances in nanoscale structures," Rev. Mod. Phys. **82**(3), 2257–2298 (2010).

[54] D. Yoo, N.-C. Nguyen, L. Martin-Moreno, D. A. Mohr, S. Carretero-Palacios, J. Shaver, J. Peraire, T. W. Ebbesen, and S.-H. Oh, "High-throughput fabrication of resonant metamaterials with ultrasmall coaxial apertures via atomic layer lithography," Nano Lett. **16**, 2040-2046 (2016).

[55] L. Luo, C. Ge, Y. Tao, L. Zhu, K. Zheng, W. Wang, Y. Sun, F. Shen, and Z. Guo, "High-efficiency refractive index sensor based on the metallic nanoslit arrays with gain-assisted materials," Nanophotonics **5** (2016).

[56] Y. Huang, X. Zhang, J. Li, L. Ma, and Z. Zhang, "Analytical plasmon dispersion in subwavelength closely spaced Au nanorod arrays from planar metal–insulator–metal waveguides," Journal of Materials Chemistry C **5**, 6079-6085 (2017).